Metallo-Organic Compounds As A smart Therapeutic Agents For Prostatic Carcinoma PC-3

Abdou S. El-Tabl[1], Reham.M.W.Faried[2], Eman .S.Nofal[1] and Mohammed H. H. Abu-Setta [*1]

[1,2]Department of Chemistry, Faculty of Science, El-Menoufia University, Shebin El- Kom, Egypt.

ABSTRACT

Metalloorganic compounds of Mn(II), Fe(III), Co(II), Ni(II), Cu(II), Zn(II) and Cd(II) of new diethyl (Z)-4-hydroxy-3-((2-((2-hydroxybenzlidene)amino)phenyl)carbamoyl) benzenesulfonic acid ligand have been synthesized and characterized using spectral analyses; (^{1}H-NMR, mass, IR, UV-VIS and ESR) , magnetic moments , conductance, XRD ,elemental and thermal analysis. Molar conductances in DMF solutions indicated that, the complexes are non-electrolytes; (5.56 - 9.51 ohm^{-1} cm^2 mol^{-1}). The ESR spectra of solid Mn(II) complex **(3)**, showed an isotropic type confirming an octahedral geometry. In addition, it was found that ESR spectrum of Co(II) Complex **(5)** at room temperature is interesting to note that $g_{\perp}$ is greater than $g_{\parallel}$, indicating a compressed tetragonal distortion along the Z-axis . However,Cu(II) complexes **(8)** and **(10)** showed an axial type symmetry indicating a $d_{(x^2-y^2)}$ ground state with a significant covalent bond character. X-ray Diffraction Spectroscopy XRD has been done. The XRD reveal that $[(H_2L)Cu(OAc)_2S].2H_2O$;Complex **(8)**, $[(H_2L)Zn(OAc)_2S].2H_2O$;Complex **(11)** and $[(H_2L)Cd(OAc)_2S].2\ H_2O$;complex **(12)** these complexes have the average crystallite sizes of 19.39, 21.77 and 22.01 nm respectively. It was suggested that the complexes are nanocrystalline.Cytotoxic evaluation of the complexes as antitumor agents against prostate cancer , PC-3 cell line has been carried out. Cu(II) complex **(8)** showed more potent cytotoxic effect against prostate cancerous cells with IC_{50}= 2.51 μg/ml .Complexes showed enhanced activity in comparison to the parent ligand and standard drug used .

Keywords:

Schiff Base ligand , complexes, analysis , , magnetism , ESR, XRD,cytotoxicity, Prostate cancer.

Introduction

The American Cancer Society estimates that there will be 248,530 new cases of prostate cancer in 2021 and more than 3.1 million prostate cancer survivors in the United States.1 The American Cancer Society also estimates that prostate cancer will be the second leading cause of cancer-related death in US men after lung cancer in 2021.1 Furthermore, rates of prostate cancer are higher in men of African descent compared with men of European descent [1]. Germline testing (genetic testing for genes linked with hereditary cancer risk) has emerged as integral to prostate cancer precision treatment in the metastatic setting, is increasingly informing screening strategies, and provides hereditary cancer information for men and their families [1]. In recent years, there has been an exponential rise in understanding the role of genetic mutations in prostate cancer predisposition and the development of new precision therapies [2]. Many genes are now incorporated into the guidelines for genetic testing to assess the risk of developing prostate cancer and offer guidance for targeted therapeutics[1-3]. In May 2020, the US Food and Drug Administration (FDA) approved 2 poly(adenosine diphosphate [ADP]-ribose) polymerase (PARP) inhibitors for the treatment of men with metastatic, castration-resistant prostate cancer (mCRPC) based on improved clinical responses [3,4]. Several challenges exist in implementing genetic testing and counseling into prostate cancer treatment paradigms. These include lack of awareness among providers regarding the utility of genetic testing for prostate cancer treatment and management, concerns around which mutations are clinically relevant, implications for at-risk family members, medical and legal liability if mutations are detected and the duty to warn, access to certified genetic counselors, financial concerns, and the time involved in obtaining a complete family history [5,6]. Additional practice challenges include a relative shortage of genetic counselors; in 2021, there are 5629 certified genetics counselors in the United States, and not all states have licensed genetic counselors [7,8]. Therefore, delivery of genetics care has necessitated that primary care providers (PCPs) have increasing working knowledge of germline testing, build collaborative models with genetic services, and consider alternate delivery of genetic information to patients through videos or telehealth [2,8,9]. Considering that men with prostate cancer, men at increased risk for prostate cancer, or prostate cancer survivors constitute a substantial proportion of patients seen by PCPs, there is a critical need to better integrate primary care with the genetic evaluation process. Metallodrugs offer many features over purely organic compounds due to specific characteristics of coordination compounds. Their bioactivity is affected by the type of central atom, its coordination and oxidation number, type and number of the ligands, coordination geometry and charge of the complex [10]. In recent years, the coordinated Chemistry of diamines have attracted the attention of researchers due to their unique capability of constructing complicated organic molecules using centers of metal as intermediates. For example, N-phenyl-ortho-phenylenediamine coordinated to platinum or nickel atoms transforms into imidazophenazine derivatives [11].The coexistence of hydrolizable ester group (-

COO-) and amide group (-NHCO-), which are capable of establishing strong intermolecular hydrogen bond interactions, becomes fundamental to obtaining a suite of materials with tailored properties. Specifically, different polyester amides have been developed for biomedical applications such as drug delivery systems [12]. Literature survey reveals that nitrogen - and sulfur-containing compounds showed very good bioactivity, being potentially active against cancer as well as viral and fungal diseases [13,14]. The amide moiety has attracted further interest because it is widespread in natural and synthetic drugs and shows lower toxicity [15]. Bioactivity of amides can also be achieved by constructing the amide with hydroxypentanedioate [16].

Experiment

Materials and Instrumentation

All the reagents employed for the preparation of the ligand and its complexes were synthetic grade and used without further purification. TLC is used to confirm the purity of the compounds. C, H, N and Cl analyses were determined at the Analytical Unit of Cairo University, Egypt. Standard gravimetric methods were used to determine metal ions [19-21]. All metal complexes were dried under vacuum over P_4O_{10}. The IR spectra were measured as KBr pellets using a PerkinElmer 683 spectrophotometer (4000-400 cm^{-1}). Electronic spectra (qualitative) were recorded on a PerkinElmer 550 spectrophotometer. The conductances (10^{-3}M) of the complexes in DMF were measured at 25°C with a Bibby conductmeter type MCl. ^{1}H-NMR spectra of the ligand and its complexes (**11,12**) were obtained with PerkinElmer R32-90-MHz spectrophotometer using TMS as internal standard. Mass spectra were recorded using JEULJMS-AX-500 mass spectrometer provided with data system. The thermal analyses (DTA and TGA) were carried out in air on a Shimadzu DT-30 thermal analyzer from 27 to 800°C at a heating rate of 10°C per minute. All XRD measurements were acquired by an FS5 spectrofluorometer (Edinburgh, UK) with a 150 W xenon lamp source for excitation. Magnetic susceptibilities were measured at 25°C by the Gouy method using mercuric tetrathiocyanatocobalt(II) as the magnetic susceptibility standard. Diamagnetic corrections were estimated from Pascal's constant. The magnetic moments were calculated from the equation: The ESR spectra of solid complexes at room temperature were recorded using a varian E-109 spectrophotometer, DPPH was used as a standard material. The TLC of all compounds confirmed their purity [22].

Prepration of ligand (1):

Prepration of 3-((2-aminophenyl)carbamoyl)-4-hydroxybenzenesulfonic acid:

3-((2-aminophenyl)carbamoyl)-4-hydroxybenzenesulfonic acid (scheme 1) was prepared by adding equimolar amount of 2-hydroxy-5-sulfobenzoic acid (30g,1mole) to benzene-1,2 diamine (14g,1mole) in 50 cm^3 of absolute ethanol. The mixture was refluxed on water bath for 2 houre and then left to cool at room tempreture , washed with water, dried and recrystallized from ethanol to afford 3-((2-aminophenyl)carbamoyl)-4-hydroxybenzenesulfonic acid.

Prepration of schiff base ligand (Z)-4-hydroxy-3-((2-((2-hydroxybenzylidene) amino) phenyl) carbamoyl) benzenesulfonic acid:

The ligand (H_2L) (Z)-4-hydroxy-3-((2-((2-hydroxybenzylidene)amino)phenyl)carbamoyl) benzenesulfonic acid (scheme 1) was prepared by adding equimolar amount of 3-((2-aminophenyl)carbamoyl)-4-hydroxybenzenesulfonic acid (14.96g,1mole) to salicyaldehyde (5.92g, 1mole) in 50 cm^3 of absolute ethanol. The mixture was stirred for Two houre [22]. After cooling, the solvent was removed under reduced pressure to give crude product which was crystallized in ethanol to yield pure ligand (1) : yield 80%, m.p. 154,color is Dark red ; Anal.calcd (%) for $C_{20}H_{16}N_2O_6$ S(FW = 412.42); C (58.25) ; H (3.91) ; N (6.79) ; S (7.77) ; Found (%) C (57.04); H (3.9); N (6.01) S (6.98). IR (KBr, cm^{-1}) 3459,3365 *V(*OH); 1635 *V*(C=O); 1600,1580 *V*(C=N); 3280,3245 *V* (N-H); 1285 *V*(COH); 1466,706 *V* $(Ar)_{para\ sub.}$; 1385,661 $(Ar)_{ortho\ sub.}$.).

Scheme 1: Preparation of ligand (Z)-4-hydroxy-3-((2-((2-hydroxybenzylidene)amino)phenyl)carbamoyl)benzenesulfonic acid

Preparation of metal complexes (2)-(12) :

The metal complexes were prepared as (1L:1M) by refluxing with stirring a suitable amount (1.0 mol) of a hot ethanolic solution of the following metal salts: (0.0.59 g ,0.002 mol) $Mn(CH_3COO).4H_2O$ complex **(2)** , (0.33 g ,0.0019 mol) Mn $SO_4 \cdot H_2O$ complex **(3)**, (0.43 g ,0.002 mol) $FeSO_4 \cdot 7H_2O$ complex**(4)**, (0.41 g, 0.0014 mole)$CoSO_4 \cdot 7H_2O$ complex **(5)**, (0.8 g ,0.0032 mol) $Ni(CH_3COO)_2 \cdot 4H_2O$ complex **(6)**, (0.5 g ,0.002 mol) $NiCl_2 \cdot 6H_2O$ complex**(7)**, (0.73 g ,0.0036 mol) $Cu(CH_3COO)_2 \cdot H_2O$ complex **(8)**, (0.22 g ,0.002 mol) $CuCO_3 \cdot 3H_2O$ complex **(9)**, (0.21 g ,0.001 mol) $CuCl_2 \cdot 2H_2O$ complex **(10)**, (0.72 g ,0.003 mol) $Zn(CH_3COO)_2 \cdot 2H_2O$ complex **(11)**, (0.64 g ,0.002 mol) $Cd(CH_3COO)_2 . 2H_2O$ complex **(12)** with a hot ethanolic solution of the ligand (1 mmol, 30 mL ethanol). The refluxing times varied

from 2 to 4 hours according to the depending to nature of metal ion. The precipitates were filtered off, washed with ethanol then by diethyl ether and dried in vacuum desiccators over P_4O_{10} [23].

Analytical data for the prepared complexes are:

Complex (2), [(H_2L) Mn $(OAc)_2$ S].2H_2O**:** Yield: 65 %; m.p. >300 ^oC; color: Orange; molar conductivity : 7.23 $ohm^{-1}cm^2mol^{-1}$.Anal.Calcd. (%)for $C_{24}H_{26}N_2O_{12}Mn$ (FW = 621.47): C, 46.1; H, 4.51; N, 4.3; S, 5.16; Mn, 8.51; Found (%) C, 46.38; H, 4.22; N, 4.51; S, 4.94 ;Mn, 8.84; IR (KBr, cm^{-1}), 3068,3015υ(NH), 1616,1547υ(C=N), 1457,749and 1382,592$\upsilon(C=C)_{Ar}$, 1245υ(C-OH) , 1660 υ(C=O) , 535 υ(M←O), 430 υ(M←N).

Complex (3), [(H_2L)Mn(SO_4)$_2$ S(H_2O)].3H_2O**:** Yield: 70 %; m.p. >300 ^oC; color: Brownish red; molar conductivity: 9.51 $ohm^{-1}cm^2mol^{-1}$.Anal.Calcd. (%)$C_{20}H_{24}N_2O_{14}S_2Mn$ (FW = 635.48): C, 37.08; H, 3.6; N,14.03; S, 9.89; Mn, 8.55; Found (%) C, 37.8; H, 3.81; N, 14.41; S,10.09; Mn, 8.65; ; IR (KBr, cm^{-1}), 3005,2926υ(NH), 1621,1580υ(C=N), 1505,748 and 1462,589 $\upsilon(C=C)_{Ar}$, 1223 υ(C-OH) , 1670 υ(C=O) , 531 υ(M←O), 472υ(M←N).

Complex (4), [(HL)Fe(SO_4) S(H_2O)].2H_2O**:** Yield: 65%; m.p.>300 ^oC; color: black; molar conductivity: 8.8 $ohm^{-1}cm^2mol^{-1}$.Anal.Calcd. (%)for $C_{20}H_{22}N_2O_{13}S_2Fe$ (FW = 618.37): C, 37.09; H, 3.46; N, 4.41; S, 10.02;Fe, 9.15; Found (%) C, 38.85; H, 3.59; N, 4.53; S,10.37; Fe, 9.03; ; IR (KBr, cm^{-1}), 3320,3100υ(NH), 1622,1540υ(C=N),1503,749 and 1461,590 $\upsilon(C=C)_{Ar}$, 1275υ(C-OH) , 1650 υ(C=O) , 540 υ(M←O), 465 υ(M←N).

Complex (5), [(H_2L)Co(SO_4)S(H_2O)].2H_2O**:** Yield: 79 %; m.p. >300 ^oC; color: Red ; molar conductivity: 8.3 $ohm^{-1}cm^2mol^{-1}$. Anal.Calc. (%)for $C_{20}H_{22}N_2O_{13}S_2Co$ (FW = 621.46): C, 38.17; H, 3.5; N, 4.3; S, 10.1; Co, 9.31; Found (%) C, 38.65; H, 3.57; N,4.5; S, 10.32; Co, 9.48; IR (KBr, cm^{-1}), 3250,3130 υ(NH), 1615,1540 υ(C=N), and 1504,751 and 1370,592 $\upsilon(C=C)_{Ar}$, 1272 υ(C-OH) , 1674υ(C=O) , 535 υ(M←O), 469 υ(M←N).

Complex (6), [(H_2L)Ni$(OAc)_2$S].2H_2O**:** Yield: 72 %; m.p. >300 ^oC; color: Redish brown; molar conductivity: 7.37 $ohm^{-1}cm^2mol^{-1}$. For Anal. Calc. (%)f or $C_{24}H_{26}N_2O_{12}S$ Ni (FW = 625.23): C, 45.76; H, 3.96; N; S, 4.99; 4.35; Ni, 9.20; Found (%) C, 46.1; H, 4.19; N, 4.48; S, 5.13; Ni, 9.39 ; IR (KBr, cm^{-1}), 3150,3010 υ(NH), 1613,1545 υ(C=N), 1461,749 and 1379,589 $\upsilon(C=C)_{Ar}$, 1259 υ(C-OH) , 1655υ(C=O) , 545 υ(M←O), 429υ(M←N).

Complex (7), [(H_2L)Ni$(Cl)_2$S].3H_2O**:** Yield: 55 %; m.p. >300 ^oC; color: Brown; molar conductivity : 7.51 $ohm^{-1}cm^2mol^{-1}$.Anal.Calcd. (%)for $C_{20}H_{22}N_2O_9S$ Cl_2Ni (FW =596.6): C, 40.73; H, 3.85; N, 4.63; S, 5.12; Ni, 9.51 ; Cl, 11.43 ; Found(%) C, 40.3;H, 3.72; N, 4.7; S,

5.38;Ni, 9.85; Cl, 11.9 ; IR (KBr, cm^{-1}),3300,3240 υ(NH), 1611,1561υ(C=N), 1503,749 and 1368,588 $\upsilon(C=C)_{Ar}$, 1280 υ(C-OH) , 1673 υ(C=O), 523 υ(M←O), 456 υ(M←N), 429 υ(M←Cl).

Complex (8), $[(H_2L)Cu(OAc)_2S].2H_2O$ **:** Yield: 80 %; m.p.>300 ^oC; color: brown; molar conductivity: 6.89 $ohm^{-1}cm^2mol^{-1}$.Anal.Calcd. (%)for $C_{24}H_{26}N_2O_{12}S$ Cu (FW = 630.08): C, 45.72; H, 4.48; N, 4.21; S, 4.95; Cu, 10.12; Found (%) C, 45.75; H, 4.16; N, 4.45; S, 5.09; Cu, 10.09; ; IR (KBr, cm^{-1}), 3192,3099υ(NH), 1608,1560 υ(C=N), 1466,751 and 1379,590 $\upsilon(C=C)_{Ar}$, 1255 υ(C-OH) , 1630 υ(C=O) , 534 υ(M←O), 462 υ(M←N).

Complex (9), $[(H_2L)Cu(CO_3)S\ (H_2O)].2H_2O$ **:** Yield: 75 %; m.p. >300 ^oC; color: brown; molar conductivity: 5.56 $ohm^{-1}cm^2mol^{-1}$.Anal.Calcd. (%)for $C_{21}H_{32}N_2O_{12}S$ Cu (FW = 590.02): C, 42.01; H, 3.6; N, 4.31; S, 5.3; Cu, 10.24; Found (%) C, 42.75; H, 3.75; N, 4.75; S, 5.43; Cu, 10.77; ; IR (KBr, cm^{-1}), 3283,3265 υ(NH), 1612,1564 υ(C=N), 1461,748 and 1376,589 $\upsilon(C=C)_{Ar}$, 1297 υ(C-OH) , 1671 υ(C=O) , 533 υ(M←O), 473 υ(M←N).

Complex (10), $[(H_2L)Cu(Cl)_2S].3H_2O$ **:** Yield: 70 %; m.p.>300 ^oC; color: black; molar conductivity : 7.68 $ohm^{-1}cm^2mol^{-1}$.Anal.Calcd. (%)for $C_{20}H_{22}N_2O_9S\ Cl_2Cu$ (FW = 600.91): C, 40.26; H, 3.50; N, 4.35; S, 5.11; Cu, 10.39; Cl , 11.61; Found (%) C, 39.97; H, 3.69; N, 4.66; S, 5.34; Cu, 10.57; Cl, 11.8; IR (KBr, cm^{-1} IR (KBr, cm^{-1}), 3310,3220 υ(NH), 1623,1544 υ(C=N), 1464,750 and 1366,593 $\upsilon(C=C)_{Ar}$, 1298 υ(C-OH) , 1663 υ(C=O) , 537 υ(M←O), 452 υ(M←N); 431 υ(M←Cl).

Complex (11), $[(H_2L)Zn(OAc)_2S].2H_2O$**:** Yield: 68 %; m.p. >300 ^oC; color: yellow; molar conductivity: 6.56 $ohm^{-1}cm^2mol^{-1}$. Anal.Calcd. (%)for $C_{24}H_{26}N_2O_{12}S$ Zn (FW = 631.92): C, 45.01; H, 3.88; N; S, 4.88; 4.27, Zn, 10.31; Found (%) C, 45.62; H, 4.15; N; S, 5.07; 4.43, Zn, 10.35; IR (KBr, cm^{-1}), 3270,3190 υ(NH), 1613,1552 υ(C=N), 1453,749 and 1380,589 $\upsilon(C=C)_{Ar}$, 1298 υ(C-OH) , 1680 υ(C=O) , 536 υ(M←O), 438 υ(M←N).

Complex (12), $[(H_2L)Cd(OAc)_2S].2H_2O$**:** Yield: 58%; m.p. >300 ^oC; color: dark gray; molar conductivity: 6.62 $ohm^{-1}cm^2mol^{-1}$. Anal.Calcd. (%)for $C_{24}H_{26}N_2O_{12}S$ Cd (FW =678.95): C, 42.03; H, 3.60; N, 3.88; S, 4.23; Cd, 16.22; Found (%) C, 42.46; H, 3.86; N, 4.13; S, 4.72; Cd, 16.56; ; IR (KBr, cm^{-1}), 3321,3265 υ(NH), 1620,1559 υ(C=N), 1480,745 and 1384,597$\upsilon(C=C)_{Ar}$, 1290 υ(C-OH) , 1680 υ(C=O) , 541 υ(M←O), 440 υ(M←N).

Biological activity

Mammalian cell lines: PC-3 (prostate carcinoma) were obtained from VACSERA Tissue Culture Unit.

Chemicals Used: Dimethyl sulfoxide (DMSO), crystal violet and trypan blue dye were purchased from Sigma (St. Louis, Mo., USA).

Fetal Bovine serum, DMEM, RPMI-1640, HEPES buffer solution, L-glutamine, gentamycin and 0.25% Trypsin-EDTA were purchased from Lonza.

Crystal violet stain (1%): It composed of 0.5% (w/v) crystal violet and 50% methanol then made up to volume with ddH_2O and filtered through a Whatmann No.1 filter paper.

Cell line Propagation:

The cells were propagated in Dulbecco's modified Eagle's medium (DMEM) supplemented with 10% heat-inactivated fetal bovine serum, 1% L-glutamine, HEPES buffer and 50µg/ml gentamycin. All cells were maintained at 37ºC in a humidified atmosphere with 5% CO_2 and were subcultured two times a week.

Cytotoxicity evaluation using viability assay: For cytotoxicity assay, the cells were seeded in 96-well plate at a cell concentration of 1×10^4 cells per well in 100µl of growth medium. Fresh medium containing different concentrations of the test sample was added after 24 h of seeding. Serial two-fold dilutions of the tested chemical compound were added to confluent cell monolayers dispensed into 96-well, flat-bottomed microtiter plates (Falcon, NJ, USA) using a multichannel pipette. The microtiter plates were incubated at 37ºC in a humidified incubator with 5% CO_2 for a period of 24 h. Three wells were used for each concentration of the test sample. Control cells were incubated without test sample and with or without DMSO. The little percentage of DMSO present in the wells (maximal 0.1%) was found not to affect the experiment. After incubation of the cells for at 37°C, for 24 h, the viable cells yield was determined by a colorimetric method [23].

In brief, after the end of the incubation period, media were aspirated and the crystal violet solution (1%) was added to each well for at least 30 minutes. The stain was removed and the plates were rinsed using tap water until all excess stain is removed. Glacial acetic acid (30%) was then added to all wells and mixed thoroughly, and then the absorbance of the plates were measured after gently shaken on Microplate reader (TECAN, Inc.), using a test wavelength of 490 nm. All results were corrected for background absorbance detected in wells without added stain. Treated samples were compared with the cell control in the absence of the tested compounds. All experiments were carried out in triplicate. The cell cytotoxic effect of each tested compound was calculated**.** The optical density was measured with

the microplate reader (SunRise, TECAN, Inc, USA) to determine the number of viable cells and the percentage of viability was calculated as [(ODt/ODc)]x100% where ODt is the mean optical density of wells treated with the tested sample and ODc is the mean optical density of untreated cells. The relation between surviving cells and drug concentration is plotted to get the survival curve of each tumor cell line after treatment with the specified compound. The 50% inhibitory concentration (IC_{50}), the concentration required to cause toxic effects in 50% of intact cells, was estimated from graphic plots of the dose response curve for each conc. using Graphpad Prism software (San Diego, CA. USA) [24].

Results and discussion

All the metal complexes are stable at room temperature, insoluble in water, not hydroscopic , partially soluble in MeOH, EtOH, $CHCl_3$ and $(CH_3)_2CO$ and completely soluble in DMF and DMSO. The analytical and physical data, spectral data are compatible with the proposed structures, Figures 1-3. The molar conductances of the complexes in 10^{-3} M DMF at 25 ^oC were in the 9.51-5.56 $ohm^{-1}cm^2mol^{-1}$ range, indicating a non-electrolytic nature. These low values commensurate the absence of any counter ions in their structure. Many attempts were made to grow a single crystal until now but unfortunately, they were failed. Reaction of the ligand **(1)** with metal salts using (1L: 1M) molar ratio in ethanol gave complexes **(2-12)**.

^{1}H-NMR spectra of the ligand (1) and complexes (11,12): The ^{1}H-NMR spectra of ligand and complexes **(11,12)** in deutrated DMSO showed peaks consistent with the proposed structure. The ^{1}H-NMR spectrum of the ligand showed chemical shift observed as singlet at 10.9 ppm which was assigned to proton of aromatic hydroxyl group. The chemical shift which appeared at 9.8 ppm was attributed to the proton of CH attached to (N-of aromatic ring); Benzylidenimin (Ar─N═CH─Ar). However, The NH secondary amide proton was observed as a singlet at 5.5 ppm. A set of signals appeared as multiples in the 6.4-7.3 ppm range, corresponding to protons of aromatic ring .The ethylene proton appears as a singlet signal at 3.4 ppm [15].By comparison the ^{1}HNMR of the ligand and the spectrum of the complexes **(11)** and **(12)**; signal was observed as a singlet at 12.8 and 13.14 ppm characteristic to the O*H* group indicating that the ligand found in the protonated form. In addition,a there is a significant downfield shift of CH attached to (N-of aromatic ring); Benzylidenimin (Ar─N═CH─Ar) proton signal at 9.9 and 9.92 ppm. Another shift appear at 5.3 ppm which relative to the free ligand clarified that the metal ions are coordinated to the amide nitrogen atom. This shift may be due to the formation of a coordination bond (N→M) [26,27] (Scheme 1).

Fig. 1: Structure representation of M(II) complexes (**2**)**,(6),(7),(8),(10),(11)** and **(12)**

Fig. 2: Structure representation of metal complexes (**3**),**(5)** and **(9)**

Fig. 3: Structure representation of metal complex (**4**)

IR spectra:

The mode of bonding between the ligand and the metal ion revealed by comparing the IR spectra of the ligand **(1)** and its metal complexes **(2)-(12)**. The ligand shows bands in the 3668-3300 and 3210-2560 cm^{-1} ranges, commensurate the presence of two types of intra- and intermolecular hydrogen bonds of OH and NH groups with imine group. Thus, the higher frequency band is associated with a weaker hydrogen bond. The v(NH) group in the complexes is shifted towards lower wave number indicating coordination through nitrogen of (-NH-) group [28,29]. However, the characteristic bands of

imines, ν(C═N), ν(C-H) and ν(N-H) were observed at 1600, 3023 and 3280 cm^{-1} respectively. Strong band appears at 1285cm^{-1} is attributed to the ν(C-OH) vibration. The bands appear at 1466 and 706 cm^{-1} range, are assigned to ν(Ar) vibration . The ν(SO_3H) group appears at 1798 cm-1. By comparing the IR spectra of the complexes **(2)-(12)** with that of the free ligand. It was found that, the position of the ν(C═N) bands of imines is shifted by 8-23 cm^{-1} range towards lower wave number in the complexes indicating coordination through nitrogen of azomethine group (CH═N). This is also confirmed by the appearance of new bands in the 473-429 cm^{-1} range, this has been assigned to the ν(M-N) and appearance of new bands in the 545-531 cm^{-1},assigned to the ν(M-O) . Complex **(4)**, show ν(C-O) band in 1650 and 1255 cm^{-1} band of (C-OH) , indicating deprotonated of (C-OH) and lowering the value of the group confirming coordinated to the metal ion [30,31]. However, complexes **(2), (3), (5), (6), (7), (8), (9), (10),(11) and (12)** show ν(C-OH) in the 1223-1298 cm^{-1} range, indicating coordination to the metal ion. The ν(C-N) group appears in the 1540-1623 cm^{-1} range. The aromatic ring to the metal ion appears in the 1366-1505 cm^{-1} and 588-751 cm^{-1} ranges [31].

Magnetic moments: The magnetic moments of the metal complexes (**2**)-(**12**) at room temperatures were shown in (Table 1). Cu(II) complexes (**8**)-(**10**) showed values in the 1.67-1.70 B.M, range corresponding to one unpaired electron in an octahedral structure. Manganese(II) complexes (**2**) and (**3**) showed values 6.22 and 6.42 B.M, indicating high spin octahedral geometry around the Mn(II) ion. Co(II) complex (**5**) showed value 4.34 B.M, indicating high spin octahedral Co(II) complex. Ni(II) complexes (**6**) and (**7**) showed value 3.21 and 2.98 B.M , indicating an octahedral Ni(II) complex. Fe(II) complex (**4**) showed value 5.73 B.M, indicating high spin octahedral geometry around the Fe(II) ion .Zn(II) complex (**11**), Cd(II) complex (**12**) showed diamagnetic property [6].

X-ray Diffraction Spectroscopy XRD pattern:

Powder X-ray Diffraction Spectroscopy XRD pattern of the Cu(II) complex **(8)**, Zn(II) complex **(11)** and Cd(II) complex **(12)** bearing CH3COO− were recorded in the range (2θ = 0–80) is shown in (Figure 4). The pattern of the metal complexes was studied to further obtain evidence about the structure of the metal complexes at wavelength 1.5406 ´Å. The XRD pattern of the Cu(II) complexes shows well defined crystalline peaks indicating that the Cu(II) ,Zn(II) and Cd(II)-Schiff base complexes were in crystalline phase. The average crystallite size of the complexes dXRD was estimated from XRD patterns by Scherer's formula: $d_{XRD} = 0.9\lambda/\beta\ (\cos\theta)$ where 'λ' is the wavelength, 'β' is the full width at half maxima and 'θ' is the diffraction angle. The XRD reveal that $[(H_2L)Cu(OAc)_2S].2H_2O$, $[(H_2L)Zn(OAc)_2S].2H_2O$ and $[(H_2L)Cd(OAc)_2S].2\ H_2O$ complexes have the average crystallite sizes of 19.39, 21.77 and 22.01 nm respectively. It suggests the complexes are nanocrystalline [32].

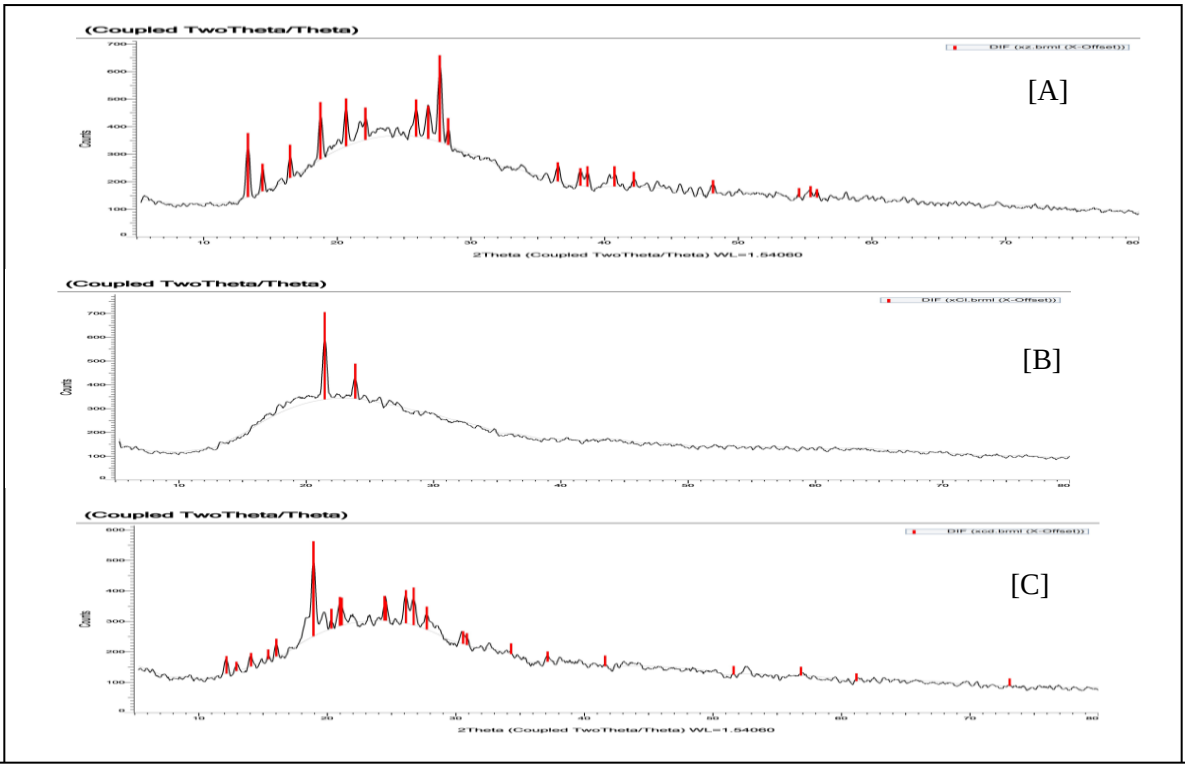

Fig. 4: X-ray Diffraction Spectroscopy XRD pattern of the Cu(II) complex (8):[A], Zn(II) complex (11);[B] and Cd(II) complex (12);[C]

Mass spectra:

The mass spectra of ligand (**1**) and its Cu(II) complex (**8**), Zn(II) complex **(11)** and Cd(II) complex (**12**) confirmed their proposed formulation. The spectrum of (**1**) reveals the molecular ion peak (m/z) at 412 amu consistent with the molecular weight of the ligand. Furthermore, the fragments observed at (m/z) = 102, 170, 224, 339 and 412 amu correspond to C_7H_2O, $C_{11}H_6O_2$, $C_{14}H_{10}NO_2$, $C_{18}H_{14}N_2O_5$, $C_{20}H_{16}N_2O_6S$ moieties respectively. Complex (**8**) shows fragments (m/z) at 146, 237, 459, 471, 497 and 630 amu due to $C_9H_6O_2$, $C_{12}H_{13}O_5$, $C_{18}H_{21}NO_{11}S$, $C_{19}H_{21}NO_{11}S$, $C_{20}H_{21}N_2O_{11}S$ and $C_{24}H_{26}CuN_2O_{12}S$ moieties respectively. The fragments observed (m /z) at 192, 263, 382, 467, 511, 589 and 631 amu for complex(**11**) were assigned to $C_{10}H_8O_4$, $C_{14}H_{15}O_5$, $C_{17}H_{18}O_{10}$, $C_{20}H_{23}N_2O_{11}$, $C_{21}H_{23}N_2O_{11}S$, $C_{22}H_{24}N_2O_{11}SZn$ and $C_{24}H_{26}N_2O_{12}SZn$ moieties, whereas the spectrum of Cd (II) complex (**12**) showed molecular ion peak at 680 assigned to the molecular weight of the complex and also showed fragments at 86, 103, 221, 300, 347, 405, 460, 523, 635 and 680 which were assigned to C_7H_2 , C_7H_3O, $C_{14}H_5O_3$,

$C_{16}H_{12}O_6$, $C_{17}H_{17}NO_7$, $C_{19}H_{20}NO_9$, $C_{21}H_{20}N_2O_{10}$, $C_{22}H_{23}N_2O_{11}S$, $C_{22}H_{23}CdN_2O_{11}S$ and $C_{24}H_{26}CdN_2O_{12}S$ moieties respectively.

Electronic spectra: The electronic spectral data for the ligand (**1**) and its metal complexes in DMF solution were summarized in (Table 1). Ligand (**1**) in DMF solution showed four bands at 315 nm ($7.60x\ 10^{-3}$ mol^{-1} cm^{-1}), 292 nm ($\varepsilon = 7.04 \times 10^{-3}$ mol^{-1} cm^{-1}) which may be assigned to $n\rightarrow\pi^*$ and $\pi\rightarrow\pi^*$ transitions of the immine and aromatic ring respectively [33]. However, Mn(II) complexes (**2**) and (**3**) showed bands in the 290-288, 390-310, 455-428 ,570-571 ranges and 615-608 nm, the first bands were within the ligand and the other bands are assigned $^6A_{1g}\rightarrow{}^4E_g$, $^6A_{1g}\rightarrow{}^4T_{2g}$ and $^6A_{1g}\rightarrow{}^4T_{1g}$ transitions which were compatible to an octahedral geometry around the Mn(II) ion [34]. Iron(III) complex (**4**) shows bands at 290,310,460,565 and 610 nm, the first two bands are within the ligand, however, the other bands are due to charge transfer and $^6A_1\rightarrow{}^4T_1$ transitions, suggesting distorted octahedral geometry around the iron(III) ion . Co(II) complex (**5**) showed bands at 285,390-312 range 462,572 and 610 nm were due to intra-ligand transitions and indicating octahedral structure , the first two bands are within the ligand and the other bands are assigned to $^4T_{1g}(F)\rightarrow{}^4T_{2g}(P)(\nu_3)$, $^4T_{1g}(F)\rightarrow{}^4A_{2g}(\nu_2)$ and $^4T_{1g}(F)$ $^4T_{2g}(F)(\nu_1)$ transitions respectively [35]. However, Ni(II) complex (**6**),(**7**) showed bands in the 282-280, 395-310, 460-440, 565-530, 610-605 and 740-735 nm ranges, the first three bands were within the ligand and the other bands are attributable to O→Ni charge transfer, $^3A_{2g}(F)\rightarrow{}^3T_{1g}(P)$ (ν_3), $^3A_{2g}(F)\rightarrow{}^3T_{1g}(F)$ (ν_2) and $^3A_{2g}(F)\rightarrow{}^3T_{2g}(F)$ (ν_1) transitions respectively, indicating an octahedral Ni(II) geometry [35,36]. The ν_2/ν_1 ratio for (**6**) and (**7**) are 1.38 and 1.31, which are less than the usual range of 1.5-1.75, indicating a distorted octahedral Ni(II) complex. Cu(II) complexes (**8**), (**9**) and (**10**) show bands in the 285 and 390-295 nm ranges , these bands are due to intraligand transitions, however, the bands appear in the 478-430, 578-565 and 610-603 nm ranges, are assigned to O→Cu, charge transfer, $^2B^1\rightarrow{}^2E$ and $^2B_1\rightarrow{}^2B_2$ transitions, indicating a distorted tetragonal octahedral structure[35,37]. Zn(II) complex (**11**) and Cd(II) complexes (**12**) showed bands due to intraligand transitions.

Table 1: Electronic spectra (nm) and magnetic moments (B.M) for the Ligand(**1**) and it complexes.

No.	λ_{max} (nm)	μ_{eff} in B.M.	$\upsilon_2 \setminus \upsilon_1$
(1)	292 ($\varepsilon = 7.04 \times 10^{-3}$ mol^{-1} cm^{-1}) 315 ($\varepsilon = 7.60x\ 10^{-3}$ mol^{-1} cm^{-1})	-	-
(2)	290,310,428,570,608	6.33	-
(3)	288,311,390,455,571,615	6.42	-
(4)	290,310,460,565,610	5.73	-

(5)	285,312,390,462,572,610	4.34	-
(6)	280,310,380,440,530,605,735	3.21	1.38
(7)	282,312,395,460,565,610,740	2.98	1.31
(8)	295,310,430,465,575,608	1.70	-
(9)	287,310,390,470,565,603	1.68	-
(10)	285,312,385,478,578,572,610	1.67	-
(11)	290,315,330	Diamag.	-
(12)	290,315,335	Diamag.	-

Electron spin resonance (ESR): The ESR spectral data for complexes **(8),(9),(10)** are presented in (Table 2). The spectra of Cu(II) complexes (**8,9,10**) are characteristic of species d^9 configuration having axial type of a $d_{(x2-y2)}$ ground state which is the most common for copper(II) complexes [34]. The complexes showed $g_{\parallel}>g_{\perp}>2.0023$, indicating octahedral geometry around copper(II) ion [38,39].The g-values are related by the expression $G = (g_{\parallel}-2)/ (g_{\perp} -2)$, where (G) exchange coupling interaction parameter (G). If G<4.0, a significant exchange coupling is present, whereas if G value > 4.0, local tetragonal axes are aligned parallel or only slightly misaligned. Complexes (**8**), (**9**) and (**10**) showed 3.33, 3.4 and 2.38 values indicating spin-exchange interactions toke place between copper(II) ions. This phenomena is further confirmed by the magnetic moments values (1.70, 1.68 and 1.67 B.M.). On the other hand, The $g_{\parallel}/A_{\parallel}$ value is also considered as a diagnostic term for stereochemistry [40]. The $g_{\parallel}/A_{\parallel}$ values for the copper complexes are 200, 217 and 156.4 cm^{-1} which lie just within the range expected for the tetragonal distorted octahedral copper(II)complexes (Table 2). The g-value of the Cu(II) complexes with a $^2B_{1g}$ ground state ($g_{\parallel}>g_{\perp}$) may be expressed by [41].

$$g_{\parallel} = 2.002 - (8K^2_{\parallel}\lambda^{\circ}/\Delta E_{xy}) \quad (1)$$

$$g_{\perp} = 2.002 - (2K^2_{\perp}\lambda^{\circ}/\Delta E_{xz}) \quad (2)$$

Where $k_{\parallel}$ and $k_{\perp}$ are the parallel and perpendicular components respectively of the orbital reduction factor (K), λ° is the spin-orbit coupling constant for the free copper, ΔE_{xy} and ΔE_{xz} are the electron transition energies of $^2B_{1g}\rightarrow{}^2B_{2g}$ and $^2B_{1g}\rightarrow{}^2E_g$. From the above relations, the orbital reduction factors ($K_{\parallel}$, $K_{\perp}$, K), which are measure terms for covalency [42], can be calculated. For an ionic environment, K=1; while for a covalent environment, K<1. The lower the value of K, the greater is the covalency.

$K^2_{\perp} = (g_{\perp} - 2.002)\ \Delta E_{xz} / 2\lambda_o$ (3)

$K^2_{\parallel} = (g_{\parallel} - 2.002)\ \Delta E_{xy} / 8\lambda_o$ (4)

$K^2 = (K_{2\parallel} + 2K^2_{\perp})/3$ (5)

K values (Table 2), for the copper(II) complexes (**8**), (**9**) and (**10**) are indicating covalent bond character [34]. Kivelson and Neiman noted that, for ionic environment $g_{\parallel} \geq 2.3$ and for a covalent environment $g_{\parallel} < 2.3$ [39]. Theoretical work by Smith seems to confirm this view. The g-values reported here (Table 2) showed considerable covalent bond character [42]. Also, the in-plane σ-covalency parameter, α^2(Cu) was calculated by

$\alpha^2\ (Cu) = (A_{\parallel}/0.036)+(g_{\parallel}-2.002)+3/7(g - 2.002)+0.04$ (6)

The calculated values (Table 2) suggested a covalent bonding [34]. The in-plane and out of- plane π-bonding coefficients β_1^2 and β^2 respectively, are dependent upon the values of ΔE_{xy} and ΔE_{xz} in the following equations [35].

$\alpha^2\beta^2 = (g_{\perp} - 2.002)\ \Delta E_{xy}/2\lambda_o$ (7)

$\alpha^2\beta_1^2 = (g_{\parallel} - 2.002)\ \Delta E_{xz}/8\lambda_o$ (8)

In this work, the complexes (**8**), (**9**) and (**10**) showed β_1^2 values 0.85, 0.88 and 0.77 indicating a moderate degree of covalency in the in-plane π-bonding [42].β^2 value for complexes (**8**), (**9**) and (**10**) showed 1.23,1.19 and 1.51 indicating ionic character of the out-of-plane, [34,43]. It is possible to calculate approximate orbital populations for d orbitals [44] by

$A_{\parallel} = A_{iso} - 2B[1 \pm (7/4)\ \Delta g_{\parallel}]\ \ \Delta g_{\parallel} = g_{\parallel} - g_e$ (9)

$\alpha_{p,d}^{\ 2} = 2B/\ 2B°$ (10)

Where A° and 2B° is the calculated dipolar coupling for unit occupancy of d orbital respectively. When the data are analyzed, the components of the [44]. Cu hyperfine coupling were considered with all the sign combinations. The only physically meaningful results are found when $A_{\parallel}$ and $A_{\perp}$ were negative. The resulting isotropic coupling constant was negative and the parallel component of the dipolar coupling 2B are negative (-206.3, -228.5 and -131 G). These results can only occur for an orbital involving the d_{x2-y2} atomic orbital on copper. The value for 2B is quite normal for copper(Il) complexes [45]. Complex (**2**),(**3**),(**4**),(**5**) showed isotropic spectra with g_{iso}= 2.03, 2.04 ,2.03, 2.02 respectively.

Table 2:-ESR data for some metal (II) complexes:-

No.	$g_{\parallel}$	$g_{\perp}$	g_{iso} [a]	$A_{\parallel}$ (G)	$A_{\perp}$ (G)	A_{iso} [b] (G)	G [c]	ΔE_{xy}	ΔE_{xz}	$K_{\perp}^2$	$K_{\parallel}^2$	K	K^2	$g_{\parallel}/A_{\parallel}$	α^2	$ß^2$	$ß_1^2$	-2 ß	a_d^2 (%)
(2)	-	-	2.03	-	-	-	-	-	-	-	-	-	-	-	-	-	-	-	-
(3)	-	-	2.04	-	-	-	-	-	-	-	-	-	-	-	-	-	-	-	-
(4)	-	-	2.03	-	-	-	-	-	-	-	-	-	-	-	-	-	-	-	-
(5)	-	-	2.02	-	-	-	-	-	-	-	-	-	-	-	-	-	-	-	-

(8)	2.2	2.06	2.11	95	5	35	3.33	17391	21505	0.75	0.52	0.91	0.84	200	0.61	1.23	0.85	206.3	87.8
(9)	2.17	2.05	2.13	115	10	45	3.4	17699	21277	0.61	0.45	0.74	0.56	217	0.51	1.19	0.88	228.5	97.2
(10)	2.19	2.08	2.12	120	15	50	2.38	17482	20920	0.98	0.5	0.90	0.82	156.4	0.65	1.51	0.77	131	56

a) $g_{iso} = (2g_{\perp} + g_{\parallel})/3$, b) $A_{iso} = (2A_{\perp} + A_{\parallel})/3$, c) $G = (g_{\parallel} - 2)/(g_{\perp} - 2)$

Thermal analyses (DTA and TGA): Since the IR spectra indicate the presence of water molecules, thermal analyses (DTA and TGA) were carried out to certain their nature. The thermal curves in the temperature 27-600°range for complexes (**3**), (**6**), (**8**), (**11**) and (**12**) are thermally stable up to 35 °C. Broken of hydrogen bonding occurs as endothermic peak within the temperature 35-45 °C range as shown in (Table 3). Dehydration is characterized by endothermic peaks within the temperature 100°C , corresponding to the loss of hydrated water molecules as in complexes (**3**) ,(**8**),(**11**)and (**12**). The elimination of coordinated water molecules occur in 200°C accompanied by endothermic peak as in complexes (**3**) [46,47]. The TG and DTA thermogram of Mn(II) complex (**3**) showed that, the complexes decomposed in five steps. The first occurred at 40°C with no weight loss as endothermic peak, may be due to break of hydrogen bonding. The second step occur at 100°C with 7.1 % weight loss (Calc. 7.3%) as endothermic peak which could be due to the elimination of three hydrated water molecules. The decomposition step which occurred at 200°C with 10.1% weight loss (Calc. 10.3%) could be due to the elimination of one coordinated H2O. The TG curve displays another thermal decomposition at 310°C with 24.3% weight loss (Calc. 24.42%), which could be due to the loss of coordinated sulphate group. The complex shows an endothermic peak observed at 405°C is due its melting point. Finally, exothermic peaks appear at 475,495,550,585 and 600 °C corresponding to oxidative thermal decomposition which proceeds slowly with leaving MnO with 23.63% weight loss (Calc. 23.81%)[72]. The TG and DTA thermogram of Ni(II) Complex (**6**) shows endothermic peak at 185 with 11.42% weight loss (Calc. 11.75%) are assigned to two hydrated water molecules. The endothermic peak observed at 315°C with 12.17% weight loss (Calc. 12.23%), could be due to the loss of coordinated acetate group. Another endothermic peak observed at 390°C with no weight loss may be due to its melting point. Finally, the complex shows exothermic peaks at 480,510,565,600 and 610°C with 23.04% weight loss (Calc. 23.15%) corresponding to oxidative thermal decomposition which proceeds slowly with final residue, assigned to NiO. The TG and DTA thermogram of Cu(II) complex (**8**) shows endothermic peak at 45°C, due to break of hydrogen bonding. Another endothermic peak appeared at 100°C, with 4.03% weight loss (Calc. 4.2%), due to loss of two hydrated water molecules. Another endothermic peak at with 11.92% weight loss (Calc. 12.05%) is due to loss of coordinated OAc group. The complex displayed another endothermic peak at 330°C may be assigned to its melting point. Oxidative thermal decomposition occurs in the 400,450,500,580 and 650°C with exothermic peaks, leaving CuO with 13.60% weight loss (Calc. 13.83%). The TG and DTA thermogram of Zn(II) complex (**11**) shows endothermic peak at 100°C with 3.95% weight loss (Calc. 4.2%) is assigned to the loss of two hydrated water molecules. Another endothermic peak at with 11.12% weight loss (Calc. 11.35%) is due to loss of coordinated OAc group. At 380°C, endothermic peak appeared which is due to melting point. Oxidative thermal decomposition occurs at 550,600,660 and 680 °C with exothermic peaks, leaving ZnO with 48.43% weight loss (Calc. 48.81%). The TG and DTA thermogram of Cd(II) complex (**12**) shows an endothermic peak at 45°C due to break of hydrogen bonding and another endothermic peak at 100 °C, with 11.55% weight loss (Calc. 11.8%) due to loss of two hydrated water molecule. The endothermic peak observed at 300°C with 20.76% weight loss (Calc. 20.34%) is due to loss of coordinated acetate group. Another

endothermic peak observed at 360°C may be assigned to its melting point. Oxidative thermal decomposition occurs at 410,460,550,600 and 650°C with exothermic peaks, leaving CdO with 35.23% weight loss (Calc. 35.4%).

Table 3:- Thermal analyses for metal (II) complexes

Compound No. Molecular formula	Temp. (°C)	DTA (peak)		TGA (Wt.loss %)		Assignments
		Endo	Exo	Calc.	Found	
Complex (3) **$[(H_2L)Mn(SO_4)_2S(H_2O)].3H_2O$** **$C_{20}H_{24}N_2O_{14}S_2Mn$**	40	endo	-	-	-	**Broken of H-bondings**
	100	endo	-	7.3	7.1	**Loss of ($3H_2O$) hydrated water molecules**
	200	endo	-	10.3	10.1	**Loss of (H_2O) coordinated water molecules**
	310	endo	-	24.42	24.3	**Loss of coordinated SO_4 group**
	405	endo	-	-	-	**Melting point**
	475,495,550,585,600	-	Exo	23.81	23.63	**Decomposition process with the formation of MnO**
Complex (6) **$[(H_2L)Ni(OAc)_2S].2H_2O$** **$C_{24}H_{26}N_2O_{12}S Ni$**	35	endo	-	-	-	**Broken of H-bondings**
	185	endo	-	11.75	11.42	**Loss of ($2H_2O$) hydrated water molecules**
	315	endo	-	12.23	12.17	**Loss of coordinated OAc group**
	390	endo	-	-	-	**Melting point**
	480,510,565,600,610	-	Exo	23.15	23.04	**Decomposition process with the formation of NiO**
Complex (8) **$[(H_2L)Cu(OAc)_2S].2H_2O$** **$C_{24}H_{26}N_2O_{12}S Cu$**	45	endo	-	-	-	**Broken of H-bondings**
	100	endo	-	4.2	4.03	**Loss of($2H_2O$) hydrated water molecules**
	300	endo	-	12.05	11.92	**Loss of coordinated OAc group**
	330	endo	-	-	-	**Melting Point**
	400,450,500,580,650	-	Exo	13.85	13.60	**Decomposition process with the formation of CuO**
Complex (11) **$[(H_2L)Zn(OAc)_2S].2H_2O$** **$C_{24}H_{26}N_2O_{12}S Zn$**	40	endo	-	-	-	**Broken of H-bondings**
	100	endo	-	4.2	3.95	**Loss of ($2H_2O$) hydrated water molecules**
	310	endo	-	11.35	11.12	**Loss of coordinated OAc group**
	380	endo	-	-	-	**Melting point**
	550,600,660,680		Exo	48.81	48.43	**Decomposition process with the formation of ZnO**
Complex (12) **$[(H_2L)Cd(OAc)_2S].2H_2O$** **$C_{24}H_{26}N_2O_{12}S Cd$**	45	endo	-	-	-	**Broken of H-bondings**
	100	endo	-	11.8	11.55	**Loss of ($2H_2O$) hydrated water molecules**
	360	endo	-	-	-	**Melting point**
	300	endo	-	20.34	20.76	**Loss of coordinated OAc group**
	410,460,550,600,650	-	Exo	35.4	35.23	**Decomposition process with the formation of CdO**

Antitumer studies

Invitro biological screening tests of the ligand and its metal complexes (2-12) were carried out as antitumor activity.The antitumor effects of the ligands (**1**) and itis metal complexes (**8**), (**11**) and (**12**) in DMSO were evaluated against PC-3 cell line. These were tested by comparing them with the standard drug (Cisplatin). The solvent DMSO showed no effect on cell growth as it reported previously [36]. The ligand shows interesting anticancer activity against PC-3 cell line at ranges of concentrations used, however, the complexes showed better effect against PC-3 cell lines. The data indicated that, complexes were active against prostate carcinoma cells . Copper complex **(8)** showed the highest cytotoxicity effect against PC-3 cell line with IC_{50} value of 2.51 µg/ml, followed by complex **(12)** with IC_{50} value 14.23 µg/ml and then complex **(11)** with IC_{50} value 44.92 µg/ml as shown in (Figure 5). The cytotoxicity of the copper complex (**8**) is more active than standard drugs used as shown in (Figure 7-11). This can be explained as Cu(II) ion binds to DNA. It seems that, changing the anion and the nature of the metal ion has effect on the biological behavior, due to alter binding ability of DNA binding, so testing of different complexes is very interesting from this point of view. Chemotherapeutic activity of the complexes may be attributed to the central metal atom which

was explained by Tweedy's chelation theory [48,44]. Also, the positive charge of the metal increases the acidity of coordinated ligand that bears protons, leading to stronger hydrogen bonds which enhance the biological activity [50,51].

Moreover, Gaetke and Chow had reported that, metal has been suggested to facilitate oxidated tissue injury through a free-radical mediated pathway analogous to the Fenton reaction [51]. By applying the ESR-trapping technique, evidence for metal - mediated hydroxyl radical formation in vivo has been obtained [52]. ROS are produced through a Fenton-type reaction as follows:

$$LM(II) + H_2O_2 \rightarrow LM(I) + .OOH + H^+$$

$$LM(I) + H_2O_2 \rightarrow LM(II) + .OH + OH^-$$

Where L, organic ligand.Also, metal could act as a double-edged sword by inducing DNA damage and also by inhibiting their repair [53]. The OH radicals react with DNA sugars and bases and the most significant and well-characterized of the OH reactions is hydrogen atom abstraction from the C4 on the deoxyribose unit to yield sugar radicals with subsequent β-elimination (Scheme 2). By this mechanism strand break occurs as well as the release of the free bases. Another form of attack on the DNA bases is by solvated electrons, probably via a similar reaction to those discussed below for the direct effects of radiation on DNA [54].

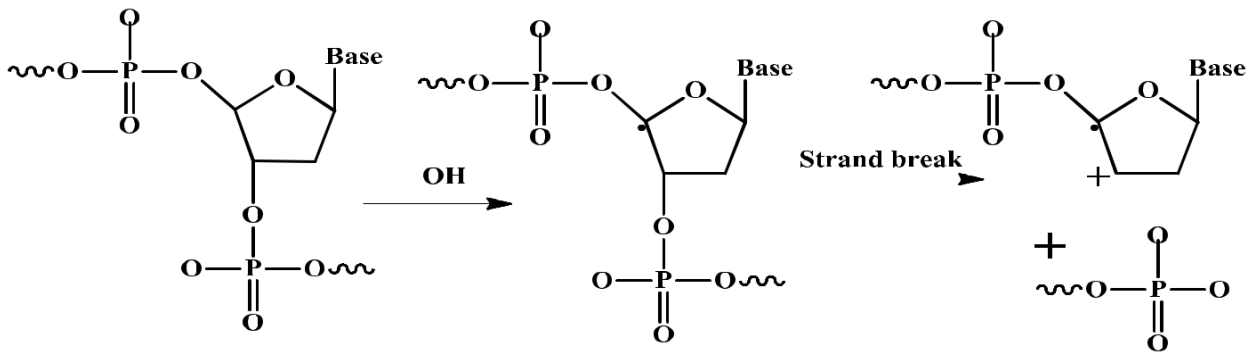

Scheme 2: Suggested mechanism for OH radicals attack on DNA sugars and bases

In the ranges of concentrations used, the chemotherapeutic effect against PC-3 cell line are depicted in (Table 4), although, the complexes have the same anions, the variable activity of the complexes may be used to oxidation – reduction potentials. The cytotoxic effect of standard drugs and metal complexes in the ranges of concentrations used against human PC-3 cell lines are shown in (Figures 6). The increase in the activity of complexes as compared to the parent ligand may be due to the complex formation in which the ligand was coordinated to the central metal ion through the nitrogen of aromatic NH_2 group with the active centers of the cell constituents resulting in an interference with the cell process leading

to an increased biological action. On comparing the results in general, it may be concluded that the complexes have greater inhibiting power than standard drug was used against all the microbes [2,6]. The zone of inhibition was measured with respect to control.

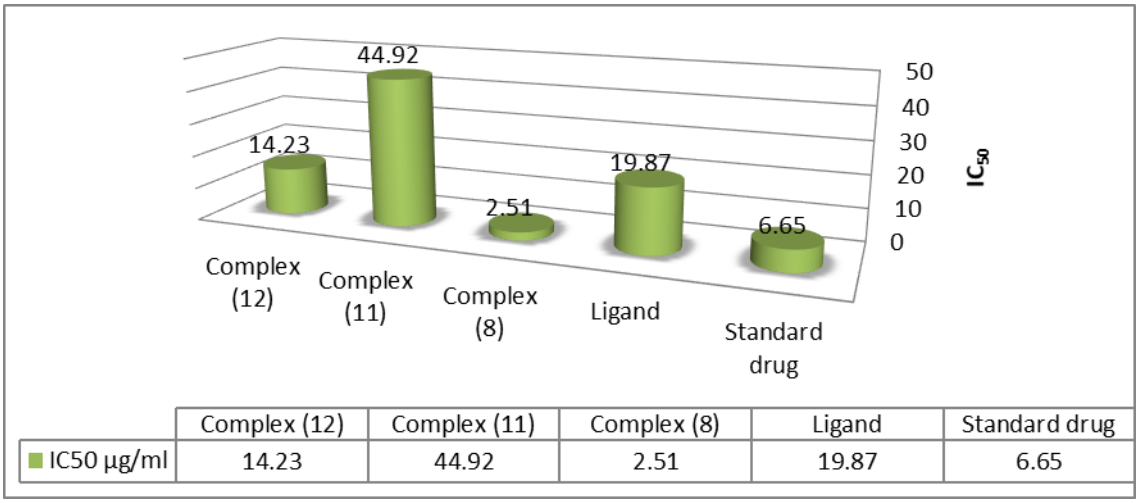

Fig. 5: IC_{50} values of the ligand, HL (**1**) and its metal complexes against human PC-3 cancer cell lines.

Table 4:- Concentrations used against PC-3 cell line

Compound	15.6 µg/ml	31.25 µg/ml	62.5 µg/ml	125 µg/ml	250 µg/ml	500 µg/ml
Ligand	45.71	61.36	73.88	85.05	92.32	97.06
Complex (8)	80.55	87.68	92.19	95.03	97.92	99.25
Complex (11)	30.66	43.22	58.71	72.82	86.06	93.27
Complex (12)	52.19	66.36	79.39	87.68	95.41	98.13

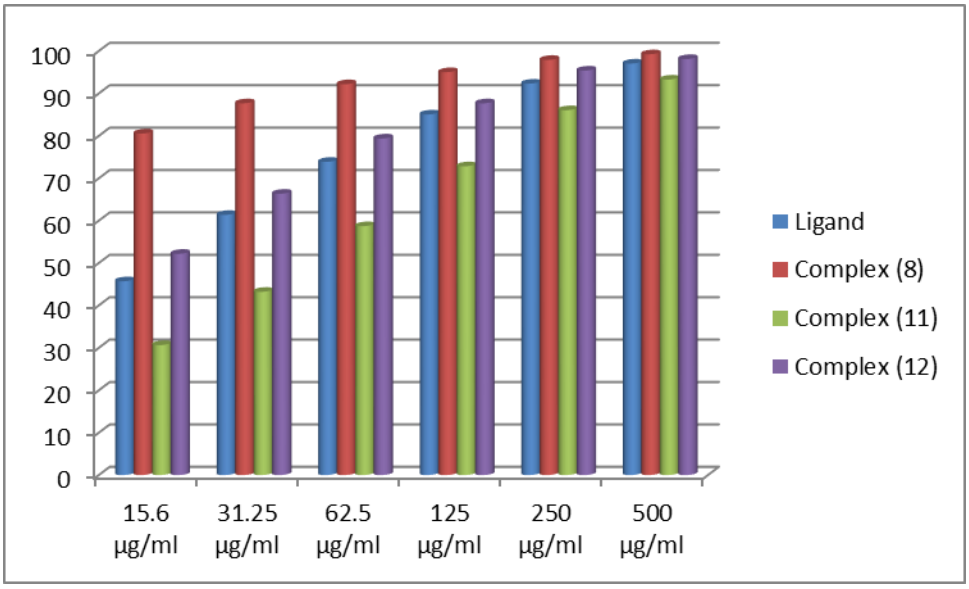

Fig. 6: Evaluation of cytotoxicity of metal complexes Against PC-3 Cell Line

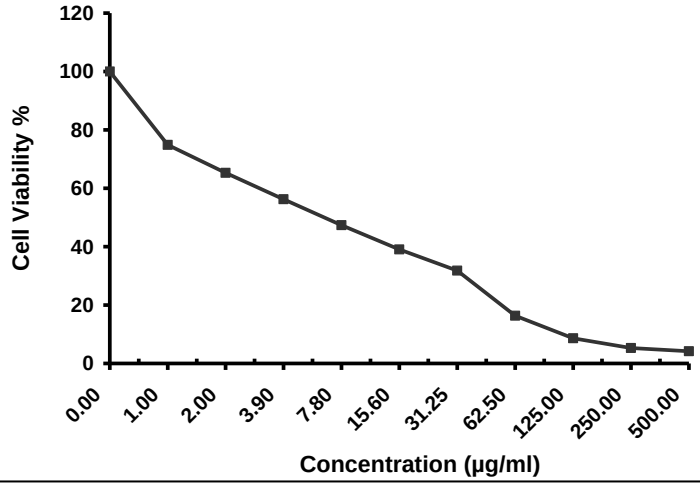

Fig. 7: Evaluation of cytotoxicity against PC-3 cell line for standard drug Cisplatin

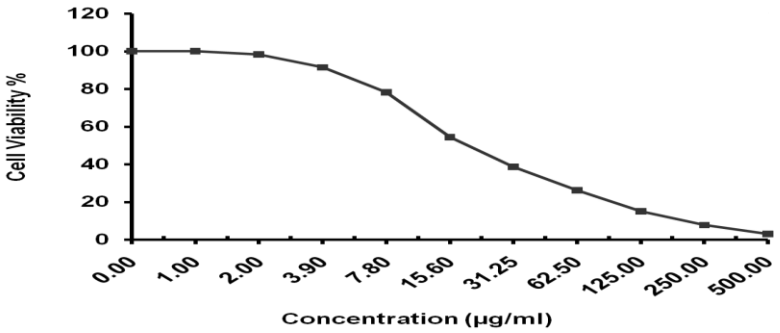

Fig. 8: Evaluation of cytotoxicity against PC-3 cell line for H_2L Ligand

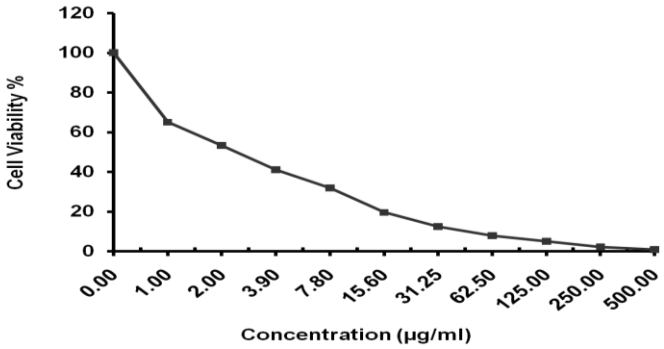

Fig. 9: Evaluation of cytotoxicity against PC-3 cell line for Cu(II) Complex (8)

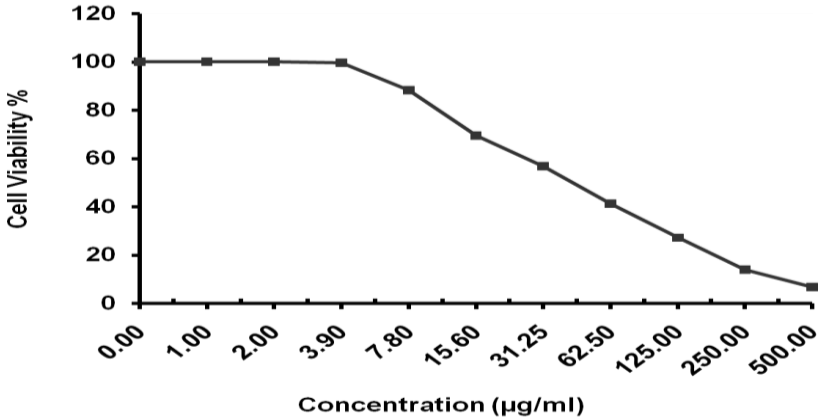

Fig. 10: Evaluation of cytotoxicity against PC-3 cell line for Zn(II) Complex (11)

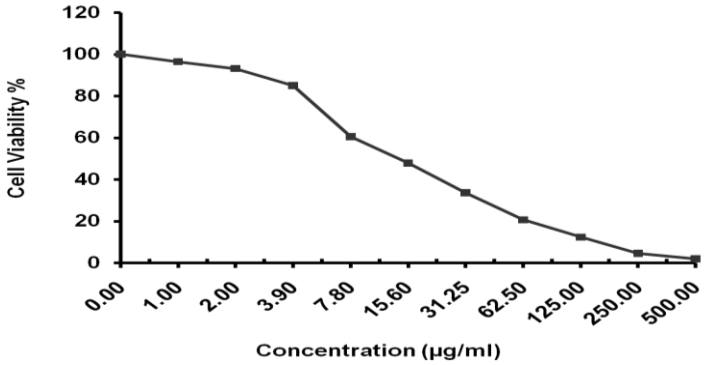

Fig. 11: Evaluation of cytotoxicity against PC-3 cell line for Cd(II) complex (12)

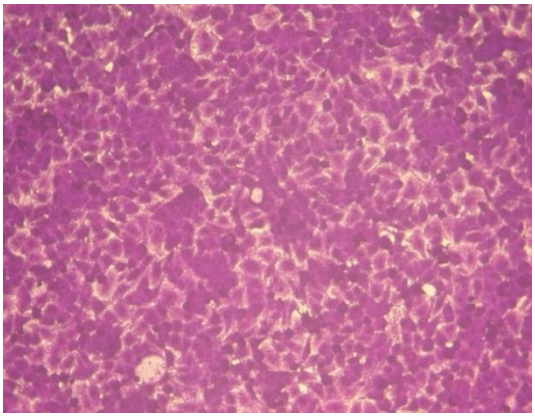

Fig. 12: PC3 cells (Non-treated control)

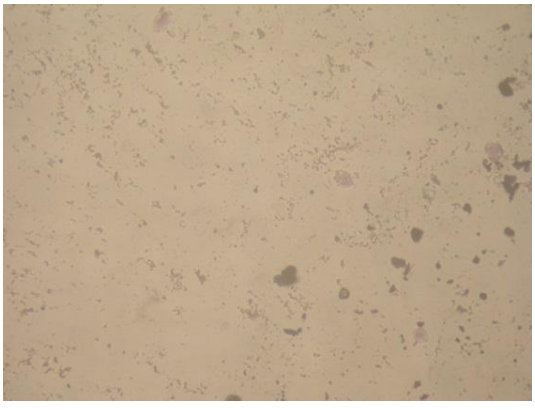

Fig. 13: PC3 cells treated with H_2L ligand (1) at conc. 500µg/ml after 24hrs.

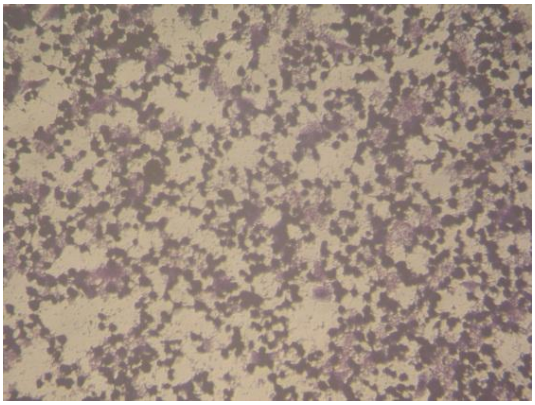

Fig. 14: PC3 cells treated with H_2L ligand (1) at conc. 100µg/ml after 24hrs.

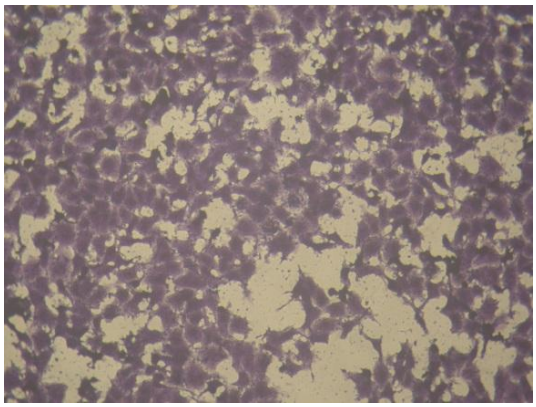

Fig. 15: PC3 cells treated with H_2L ligand (1) at conc. 20µg/ml after 24hrs.

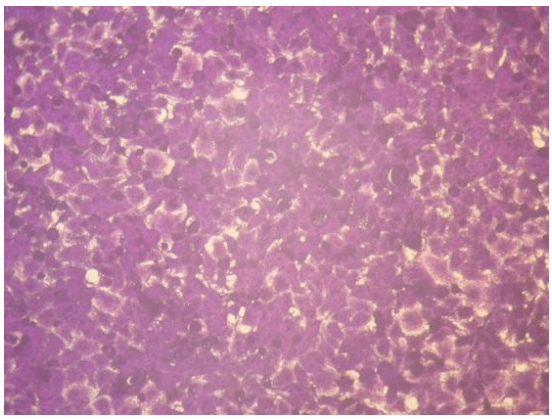

Fig. 16: PC3 cells treated with H_2L ligand (1) at conc. 4µg/ml after 24hrs.

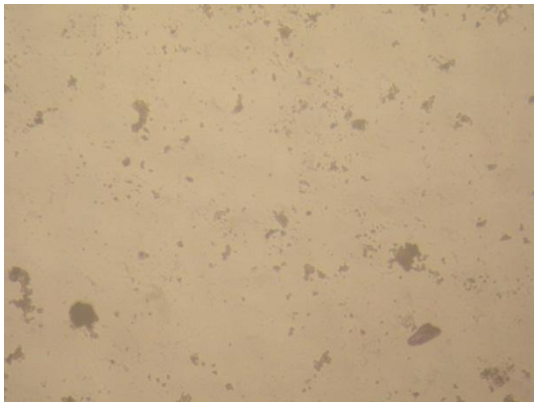

Fig. 17: PC3 cells treated with Cu(II) complex (8) at conc. 500µg/ml after 24hrs.

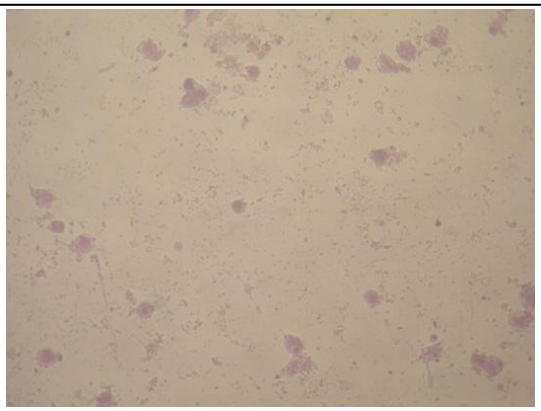

Fig. 18: PC3 cells treated with Cu(II) complex (8) at conc. 100µg/ml after 24hrs.

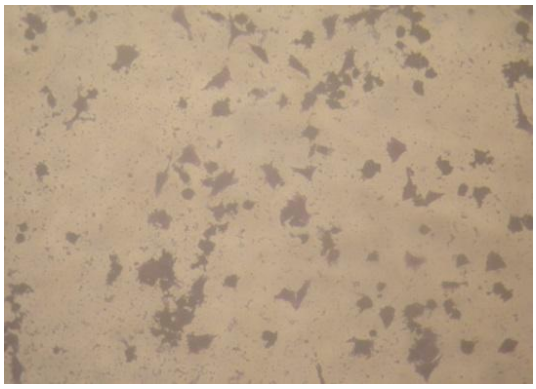

Fig. 19: PC3 cells treated with Cu(II) complex (8) at conc. 20µg/ml after 24hrs.

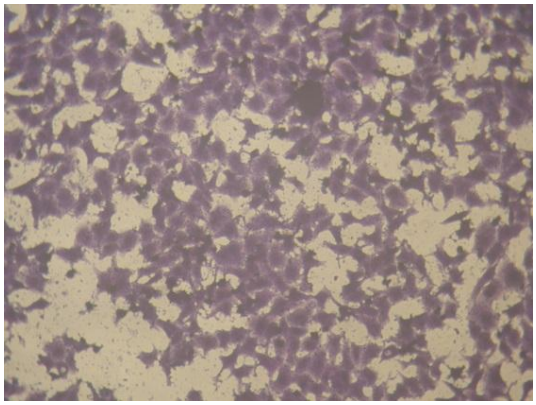

Fig. 20: PC3 cells treated with Cu(II) complex (8) at conc. 4µg/ml after 24hrs.

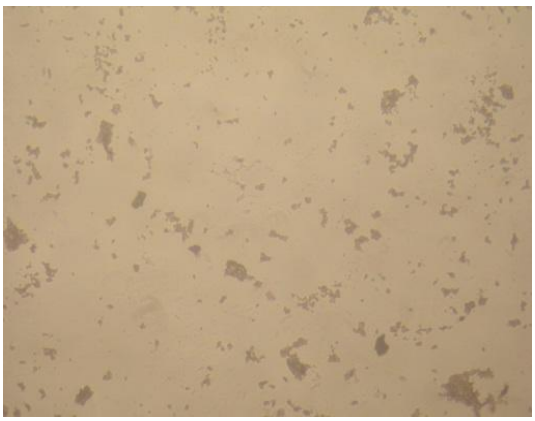

Fig. 21: PC3 cells treated with Cd(II) complex (12) at conc. 500µg/ml after 24hrs.

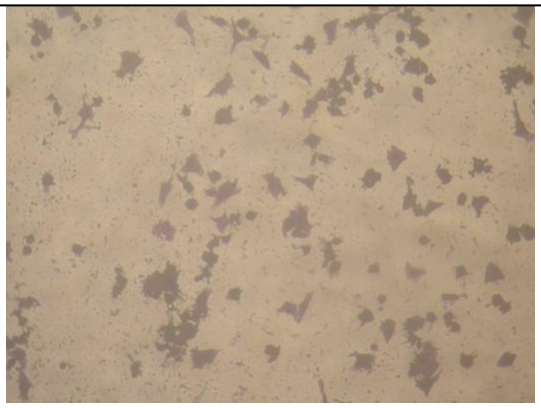

Fig. 22: PC3 cells treated with Cd(II) complex (12) at conc. 100µg/ml after 24hrs.

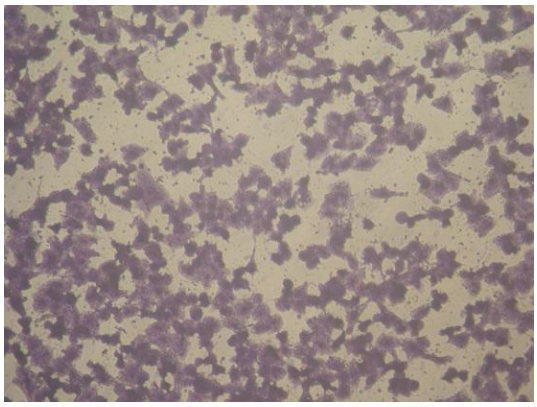

Fig. 23: PC3 cells treated with Cd(II) complex (12) at conc. 20µg/ml after 24hrs.

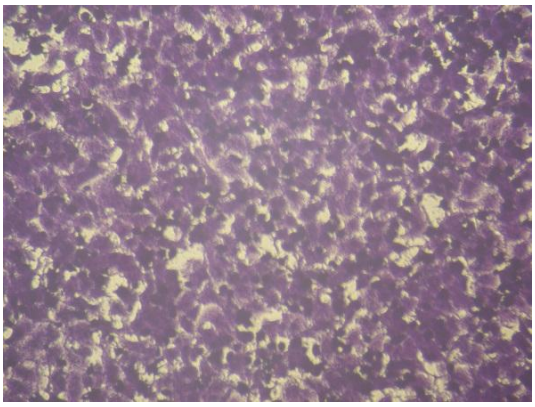

Fig. 24: PC3 cells treated with Cd(II) complex (12) at conc. 4µg/ml after 24hrs.

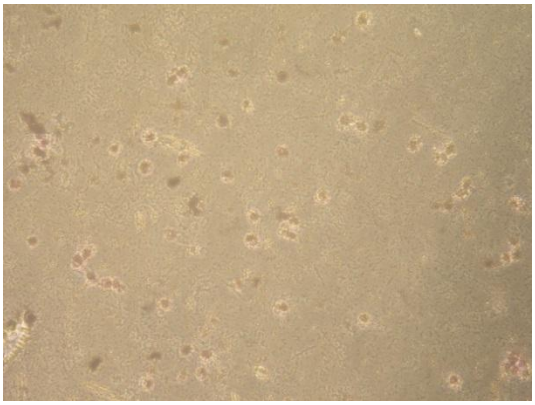

Fig. 25: PC3 cells treated with Zn(II) complex (11) at conc. 500µg/ml after 24hrs.

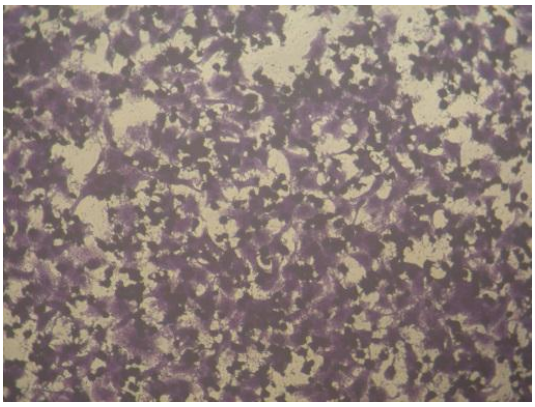

Fig. 26: PC3 cells treated with Zn(II) complex (11) at conc. 100µg/ml after 24hrs.

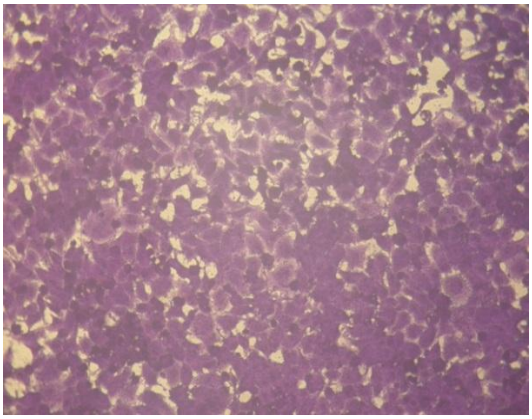

Fig. 27: PC3 cells treated with Zn(II) complex (11) at conc. 20µg/ml after 24hrs.

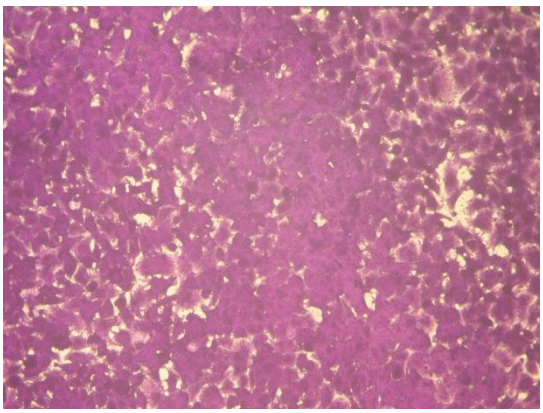

Fig. 28: PC3 cells treated with Zn(II) complex (11) at conc. 4µg/ml after 24hrs.

Conclusion

Compounds of metalloorganic Mn(II), Fe(III), Co(II), Ni(II), Cu(II), Zn(II) and Cd(II) of new diethyl (Z)-4-hydroxy-3-((2-((2-hydroxybenzlidene)amino)phenyl)carbamoyl) benzenesulfonic acid ligand have been synthesized and characterized using spectral analyses; (^{1}H-NMR, mass, IR, UV-VIS and ESR) , magnetic moments , conductance, XRD ,elemental and thermal analysis. Molar conductances in DMF solutions indicated that, the complexes are non-electrolytes; (5.56 - 9.51 ohm^{-1} cm^2 mol^{-1}). The ESR spectra of solid Mn(II) complex **(3)**, showed an isotropic type confirming an octahedral geometry. X-ray Diffraction Spectroscopy XRD has been done. The XRD reveal that $[(H_2L)Cu(OAc)_2S].2H_2O$;Complex **(8)**, $[(H_2L)Zn(OAc)_2S].2H_2O$;Complex **(11)** and $[(H_2L)Cd(OAc)_2S].2\ H_2O$;complex **(12)** these complexes have the average crystallite sizes of 19.39, 21.77 and 22.01 nm respectively. It was suggested that the complexes are nanocrystalline.Cytotoxic evaluation of the complexes as antitumor agents against prostate cancer , PC-3 cell line has been carried out. Cu(II) complex **(8)** showed more potent cytotoxic effect against prostate cancerous cells with IC_{50}= 2.51 μg/ml These organometallic compounds candidates as anti prostate cancer agents.

Funding:

This research received no external funding.

Acknowledgments

We thank the laboratory of materials and renewable energy and the central laboratory, Faculty of Science, Menofia University for doing UV measurements.

Conflicts of Interest

The authors declare no conflict of interest.

REFRANCES

[1] Giri, Veda N., et al. "Genetic testing in prostate cancer management: Considerations informing primary care." *CA: A Cancer Journal for Clinicians* 72.4 (2022): 360-371.

[2] Giri, Veda N., et al. "Implementation of germline testing for prostate cancer: Philadelphia Prostate Cancer Consensus Conference 2019." *Journal of Clinical Oncology* 38.24 (2020): 2798.

[3] Abida, Wassim, et al. "Rucaparib in men with metastatic castration-resistant prostate cancer harboring a BRCA1 or BRCA2 gene alteration." *Journal of Clinical Oncology* 38.32 (2020): 3763.

[4] de Bono, Johann, et al. "Olaparib for metastatic castration-resistant prostate cancer." *New England Journal of Medicine* 382.22 (2020): 2091-2102.
Concepcion, Raoul S. "Germline testing for prostate cancer: community urology perspective." *Can J Urol* 26.5 suppl 2 (2019): 50-51.

[5] Paller, Channing J., et al. "Germline genetic testing in advanced prostate cancer; practices and barriers: survey results from the Germline Genetics Working Group of the Prostate Cancer Clinical Trials Consortium." *Clinical genitourinary cancer* 17.4 (2019): 275-282.

[6] Resta, Robert, et al. "A new definition of genetic counseling: National Society of Genetic Counselors' task force report." *Journal of genetic counseling* 15 (2006): 77-83.

[7] Giri, Veda N., Colette Hyatt, and Leonard G. Gomella. "Germline testing for men with prostate cancer: navigating an expanding new world of genetic evaluation for precision therapy and precision management." *Journal of clinical oncology: official journal of the American Society of Clinical Oncology* 37.17 (2019): 1455-1459.

[8] Russo, Jessica, et al. "Pretest genetic education video versus genetic counseling for men considering prostate cancer germline testing: a patient-choice study to address urgent practice needs." *JCO Precision Oncology* 5 (2021): 1377-1386.

[9] Woyda-Ploszczyca, Andrzej M. "Direct and indirect targets of carboxyatractyloside, including overlooked toxicity toward nucleoside diphosphate kinase (NDPK) and mitochondrial H+ leak." *Pharmaceutical Biology* 61.1 (2023): 372-390.

[10] Nikolaevskii, S. A., et al. "Atmospheric Oxygen Influence on the Chemical Transformations of 4, 5-Dimethyl-1, 2-Phenylenediamine in the Reactions with Copper (II) Pivalate." *Russian Journal of Coordination Chemistry* 45 (2019): 273-287.

[11] Han, Shuyan, and Jun Wu. "Recent advances of poly (ester amide) s-based biomaterials." *Biomacromolecules* 23.5 (2022): 1892-1919.

[12] Devi, Jai, Binesh Kumar, and Bharti Taxak. "Recent advancements of organotin (IV) complexes derived from hydrazone and thiosemicarbazone ligands as potential anticancer agents." *Inorganic Chemistry Communications* (2022): 109208.

[13] John, Liji, et al. "Protein binding and cytotoxicity activities of glutamine based metal complexes." *Journal of Molecular Structure* 1240 (2021): 130540.

[14] El Tabl, Abdou, et al. "Modulation of cancer therapy using nano-organometallic compounds: preparation, spectroscopic characterization and cytotoxic evaluation." *Egyptian Journal of Chemistry* 64.7 (2021): 3873-3887.

[15] Egharevba, Godshelp O., et al. "Synthesis and characterization of novel combretastatin analogues of 1, 1-diaryl vinyl sulfones, with antiproliferative potential via in-silico and in-vitro studies." *Scientific Reports* 12.1 (2022): 1901.

[16] Soares da Silva Burato, Juliana, et al. "Recent advances and trends in miniaturized sample preparation techniques." *Journal of separation science* 43.1 (2020): 202-225.

[17] Mostafa, Eman A., et al. "A Turn-On–Type Fluorescence Resonance Energy Transfer Eco-friendly Method for Nitazoxanide Quantification in Pharmaceutical Dosage Form and Spiked Plasma: Evaluation of Greenness Profile Using Different Assessment Tools." *Journal of Fluorescence* (2022): 1-13.

[18] Durgaprasad Kemisetti, Mr, and Amrit Kumar Rath. "A Critical Review on Bioanalytical Methods Impurity Profiling, Degradation Study of Empagliflozin and Linagliptin." *Journal of Pharmaceutical Negative Results* (2023): 3831-3841.

[19] Capano, Giliberto, and Michael Howlett. "The knowns and unknowns of policy instrument analysis: Policy tools and the current research agenda on policy mixes." *Sage Open* 10.1 (2020): 2158244019900568.

[20] Varshochi, Mojtaba, et al. "In Vitro Susceptibility Testing of Rifampin Against Acinetobacter Baumannii: Comparison of Disk Diffusion, Agar Dilution, and E-test." *Erciyes Medical Journal* 41.4 (2019): 364-369.

[21] El-Tabl, Abdou Saad, et al. "Anticancer Agents; Synthesis, Structural Characterization of Novel Di-hydrazone Ether Complexes and Study their Anticancer Activities."

[22] Abdou, S., Moshira M. Abd-El Wahed, and Mohammed HH Abu-Setta. "Metallo-bioactive compounds as potential novel anticancer therapy." *International Journal of Advances in Chemistry* 4.1 (2018): 17-37.

[23] Takeuchi, Hitoshi, Masanori Baba, and Shiro Shigeta. "An application of tetrazolium (MTT) colorimetric assay for the screening of anti-herpes simplex virus compounds." *Journal of virological methods* 33.1-2 (1991): 61-71.

[24] ethylidene hydrazino-thiazole derivatives: A novel heterocyclic system." *Applied Sciences* 11.19 (2021): 8908.

[25] Maurya, Mannar R., and Naveen Kumar. "Chloromethylated polystyrene cross-linked with divinylbenzene and grafted with vanadium (IV) and vanadium (V) complexes having ONO donor ligand for the catalytic activity." *Journal of Molecular Catalysis A: Chemical* 383 (2014): 172-181.

[26] Nica, Simona, et al. "Vanadium (V) complex with Schiff-base ligand containing a flexible amino side chain: Synthesis, structure and reactivity." *Journal of Inorganic Biochemistry* 147 (2015): 193-203.

[27] El-Tabl, Abdou Saad, Fathey A. El-Saied, and Ahmed Noman Al-Hakimi. "Synthesis, spectroscopic investigation and biological activity of metal complexes with ONO trifunctionalalized hydrazone ligand." *Transition Metal Chemistry* 32.6 (2007): 689-701.

[28] El-Tabl, Abdou S., Mohamad ME Shakdofa, and Ahmed El-Seidy. "Synthesis, Characterization and ESR Studies of New Copper (II) Complexes of Vicinal Oxime Ligands." *Journal of the Korean Chemical Society* 55.4 (2011): 603-611.

[29] Ateş D, Gulcan M, Gümüş S, Şekerci M, Özdemir S, Şahin E, Çolak N. Synthesis of bis (thiosemicarbazone) derivatives: Definition, crystal structure, biological potential and computational analysis. Phosphorus, Sulfur, and Silicon and the Related Elements. 2018 2;193(1):14-22.

[30] El-Tabl, A., et al. "Sythesis and characterization of novel copper (II) complexes of dehydroacetic acid thiosemicarrbazone." *Polish Journal of Chemistry* 73.2 (1999): 245-254.

[31] Alorini, Thamer, et al. "An experimental and theoretical investigation of antimicrobial and anticancer properties of some new Schiff base complexes." *Research on Chemical Intermediates* 49.4 (2023): 1701-1730.

[32] Devi, Priyanka, Kiran Singh, and Bhagavati Kubavat. "Synthesis, spectroscopic, quantum, thermal and kinetics, antibacterial and antifungal studies: Novel Schiff base 5-methyl-3-((5-bromosalicylidene) amino)-pyrazole and its transition metal complexes." *Results in Chemistry* 5 (2023): 100813.

[33] El-Tabl, Abdou Saad, Moshira Mohamed Abd El-wahed, and Samar Ebrahim Abd El-Razek. "Preparation, spectroscopic investigation and antiproliferative capacity of new metal complexes of (3E)-2-(hydroxyimino)-NP-Tolyl-3-(P-tolylimino) butanamide." *Spectrochimica Acta Part A:*

Molecular and Biomolecular Spectroscopy 105 (2013): 600-611.

[34] El-Tabl, Abdou Saad, and Saeyda Abdou El-Enein. "Reactivity of the new potentially binucleating ligand, 2-(acetichydrazido-N-methylidene-α-naphthol)-benzothiazol, towards manganese (II), nickel (II), cobalt (II), copper (II) and zinc (II) salts." *Journal of Coordination Chemistry* 57.4 (2004): 281-294.

[35] Thakkar, N. V., and S. Z. Bootwala. "Synthesis and characterization of binuclear metal complexes derived from some isonitrosoacetophenones and benzidine." (1995).

[36] Sallam, Shehab A., et al. "Copper, nickel and cobalt complexes of Schiff-bases derived from β-diketones." *Transition Metal Chemistry* 27 (2002): 447-453.

[37] El-Boraey, H., and A. S. El-Tabl. "Supramolecular copper (II) complexes with tetradentate ketoenamine ligands." *Polish Journal of Chemistry* 77.12 (2003): 1759-1775.

[38] El-Tabl, Abdou Saad. "An esr study of copper (II) complexes of N-h

[39] Nikles, D. E., M. J. Powers, and F. L. Urbach. "Copper (II) complexes with tetradentate bis (pyridyl)-dithioether and bis (pyridyl)-diamine ligands. Effect of thio ether donors on the electronic absorption spectra, redox behavior, and EPR parameters of copper (II) complexes." *Inorganic Chemistry* 22.22 (1983): 3210-3217.

[40] Ray, R. K., and George B. Kauffman. "An EPR Study of some copper (II) coordination compounds of substituted biguanides. Part IV." *Inorganica chimica acta* 174.2 (1990): 257-262.

[41] Goodgame, David ML, Michael A. Hitchman, and Bernhard Lippert. "Ligating properties of platinum (II) ions in mixed-metal (Pt2M) trimers (M= copper (II), nickel (II), cobalt (II), iron (II))." *Inorganic Chemistry* 25.13 (1986): 2191-2194.

[42] Bhadbhade, M., and D. Srinivas. "Erratum to document cited in CA119 (26): 285036b." *Inorg. Chem* 32 (1993): 2458.

[43] Janes, Robert, and Martyn CR Symons. "Radical cation of HP (O)(OMe) 2: electron paramagnetic resonance evidence for competition between bonding to solvent, a 1, 2-hydrogen shift, and a 1, 4-hydrogen shift." *Journal of the Chemical Society, Faraday Transactions* 86.12 (1990): 2173-2177.

[44] Raman, Natarajan, and Thiravidamani Chandrasekar. "Metallonucleases encompassing curcumin, 2-aminobenzothiazole and o-phenylenediamine: a search for new metallonucleases." *Inorganic and Nano-Metal Chemistry* (2021): 1-13.

[45] El-Tabl, Abdou Saad, and Sanaa Mostafa Imam. "New copper (II) complexes produced by the template reaction of acetoacetic-2-pyridylamide and amino-aliphatic alcohols." *Transition Metal Chemistry* 22.3 (1997): 259-262..

[46] Bano, Nausheen, et al. "Pharmacologically bio-relevant N-functionalized homo-binuclear macrocyclic complexes: Synthesis, spectral studies, biological screening, HSA binding, and molecular docking." *Inorganic and Nano-Metal Chemistry* 49.12 (2019): 413-430.

[47] Abdou, S., et al. "Journal of Chemical, Biological and Physical Sciences."

[48] Hall, Iris H., et al. "Cytotoxicity of metallic complexes of furan oximes in murine and human tissue cultured cell lines." *Applied organometallic chemistry* 11.7 (1997): 565-575.

[49] Feng, Guoqiang, et al. "A highly reactive mononuclear Zn (II) complex for phosphodiester cleavage." *Journal of the American chemical society* 127.39 (2005): 13470-13471.

[50] Zhang, Xuepeng, et al. "Mechanismic investigation on the cleavage of phosphate monoester catalyzed by unsymmetrical macrocyclic dinuclear complexes: the selection of metal centers and the intrinsic flexibility of the ligand." *Inorganic Chemistry* 53.7 (2014): 3354-3361.

[51] Nikles, D. E., M. J. Powers, and F. L. Urbach. "Copper (II) complexes with tetradentate bis (pyridyl)-dithioether and bis (pyridyl)-diamine ligands. Effect of thio ether donors on the electronic

absorption spectra, redox behavior, and EPR parameters of copper (II) complexes." *Inorganic Chemistry* 22.22 (1983): 3210-3217.

[52] El-Tabl, Abdou S., et al. "Bimetallic transition metal complexes of 2, 3-dihydroxy-N', N'4-bis ((2-Hydroxynaphthalen-1-yl) methylene) succinohydrazide ligand as a new class of bioactive compounds; synthesis, characterization and cytotoxic evaluation." *Indian Journal of Advances in Chemical Science* 4.1 (2016): 114-129.

[53] Zoutendijk, Sebastiaan L. *LIghts in a sea of darkness: constraining the nature and properties of dark matter using the stellar kinematics in the centres of ultra-faint dwarf galaxies*. Diss. Leiden University, 2022.

Corresponding author : **Mohammed H. H. Abu-Setta**

Department of Chemistry, Faculty of Science, El-Menoufia University, Shebin El- Kom, Egypt.

Email: **drmohammedhosnyabusetta@gmail.com**